A transcriptome-wide meta-analysis reveals lack of cancer-cell intrinsic determinants of response to immune checkpoint blockade

Yu Amanda Guo[1], Tanmay Kulshrestha[1], Mei Mei Chang[1], Irfahan Kassam[1], Egor Revkov[1,2], Simone Rizzetto[1], Aaron C. Tan[3], Daniel S.W. Tan[1,3], Iain Beehuat Tan[1,3] & Anders Jacobsen Skanderup[1,2,3]

[1]Genome Institute of Singapore (GIS), Agency for Science, Technology and Research (A*STAR), 60 Biopolis Street, Genome, Singapore 138672, Republic of Singapore

[2]School of Computing, National University of Singapore, Computing 1, 13 Computing Drive, Singapore 117417, Republic of Singapore

[3]National Cancer Centre Singapore, Singapore 168583, Republic of Singapore.

Correspondence should be addressed to A.J.S. (skanderupamj@gis.a-star.edu.sg)

Declaration of interests

The authors declare no competing interests.

Abstract

Immune-checkpoint therapy (ICT) has conferred significant and durable clinical benefit to some cancer patients. However, most patients do not respond to ICT, and reliable biomarkers of ICT response are needed to improve patient stratification. Here, we performed a transcriptome-wide meta-analysis across 1,486 tumors from ICT-treated patients and tumors with expected ICT outcomes based on microsatellite status. Using a transcriptome deconvolution approach, we inferred cancer and stroma-specific gene expression differences and identified cell-type specific features of ICT response across cancer types. Consistent with current knowledge, stromal expression of *CXCL9*, *CXCL13*, *IFNG,* and *CD274* were among the top positive determinants of ICT response. Interestingly, we also identified a group of potential immune-suppressive genes, including *FCER1A*, associated with poor response to ICT. Surprisingly, the unbiased transcriptome-wide analysis failed to identify cancer-cell intrinsic features of ICT response conserved across tumor types. Overall, our results suggest that cancer cells lack tissue-agnostic molecular determinants of ICT response, which has implications for the development of improved ICT diagnostics and treatments.

37 **Introduction**

38 Immune checkpoint blockade therapy (ICT) is an established class of immunotherapy that
39 induces significant tumor shrinkage and long-term disease control in many cancers.
40 However, only a subset of patients benefit from ICT, with response rates ranging from 0-3%
41 in pancreatic cancer[1] to about 40% in melanoma and microsatellite instable (MSI) tumors[2].
42 Presently, the Food and Drug Administration (FDA)-approved biomarkers for ICT are PD-L1
43 expression[3], microsatellite instability[4], and high tumor mutation burden (TMB)
44 of >10mutations/Mb[5]. While PD-L1 expression is an obvious biomarker for PD-1/PD-L1
45 blockade therapies, it is only weakly predictive of treatment response in many solid cancer
46 types[6]. TMB is a measure of tumor immunogenicity, where increased mutation load is
47 associated with higher neo-antigen burden and anti-tumoral immune responses. However,
48 the predictive power of TMB varies significantly by cancer type and it is difficult to define a
49 single TMB threshold across cancer types[7,8]. Likewise, MSI tumors are more immunogenic,
50 as defective mismatch repair results in large numbers of insertions and deletions in the
51 cancer genomes. In practice, MSI status has limited applications as a biomarker of ICT
52 response, since only a small subset of solid tumors are microsatellite instable[9,10].

53 Transcriptional signatures of tumor immune phenotypes have been proposed to
54 predict for ICT response[11-13]. However, a recent analysis using large-scale ICT trial data
55 found that existing transcriptional signatures often have limited predictive accuracy in new
56 patient cohorts[6]. A recent meta-analysis evaluating existing biomarkers of ICT response,
57 identified TMB and *CXCL9* expression as the most consistent predictors of ICT response.
58 Despite these efforts, there is a lack of transcriptome-wide studies to identify potential
59 biomarkers of ICT response conserved across cancer types.

60 Activation of effector immune cells such as T-cells and natural killer (NK) cells are
61 dependent on a balance of co-stimulatory and co-inhibitory interactions between these
62 effector cells, antigen-presenting immune cells such as dendritic cells and macrophages, as
63 well as cancer cells in the TME. Dysregulation of these ligand-receptor interactions, or
64 immune checkpoints, leads to immunosuppression in the tumor. However, it is challenging
65 to tease apart these complex interactions between cancer and immune cells using bulk
66 tumor transcriptomics. For example, although inhibitory immune checkpoint ligand PD-L1 is
67 a known biomarker of ICT response, it is unclear if cancer cells escape immune cell killing by
68 expressing PD-L1, or recruiting PD-L1^{+} immune cells, with studies supporting both
69 scenarios[14]. Therefore, learning the cell type specificities of ICT biomarkers will shed insights
70 on the underlying mechanisms of immune evasion and ICT resistance. While single-cell
71 transcriptomics has been applied to explore immune cell types and molecular mechanisms
72 associated with ICT response, single cell transcriptomics studies are currently limited to
73 small patient cohorts[15,16]. The small sample size, coupled with high intra- and inter- patient
74 heterogeneity and intrinsic noise in single-cell data, limits the power of single-cell
75 transcriptomics for systematic biomarker discovery.

76 Here, we performed a meta-analysis on the complete transcriptomes of 534 tumors
77 from four ICT treated patient cohorts, as well as 952 ICT responder-enriched (MSI) and non-
78 responder-enriched [microsatellite stable (MSS)] tumors (**Figure 1A**). We applied a novel
79 transcriptome deconvolution technique to estimate stroma- and cancer-cell-specific
80 differential expression of individual genes from the bulk tumor transcriptomes[17]. Based on
81 the hypothesis that ICT responsive tumors share molecular features regardless of tumor
82 type, we searched for stroma and cancer-cell gene expression signatures associated with ICT
83 response across distinct cohorts and tumor types. Strikingly, our analysis revealed a lack of

84 cancer-cell intrinsic gene expression signatures associated with ICT response across tumor
85 types. In contrast, in stromal cells, we identified multiple immunomodulators and
86 checkpoint genes recurrently associated with ICT response across cohorts and tumor types.
87 While many of these genes have previously been linked with ICT response, we also
88 identified a subset of novel and potentially immune-suppressive genes negatively correlated
89 with response. Using these conserved stromal-specific gene signatures, we developed a
90 predictive model of ICT response that demonstrated improved accuracy over existing
91 biomarkers in unseen patient cohorts and tumor types.
92
93

Results

Patient cohorts used for transcriptome-wide analysis of ICT response

To systematically explore transcriptome-wide biomarkers of ICT response, we obtained transcriptome data for 534 tumors, comprising 4 ICT-treated patient cohorts from 3 tumor types (gastric cancer[18], urothelial cancer[19] and melanoma[20,21]; **Figure 1** and **Methods**). Since about half of MSI tumors are expected to respond to ICT, as compared to <10% in microsatellite stable (MSS) tumors[2,22,23], we further supplemented the discovery cohort using large cohorts of treatment-naïve MSI/MSS tumors. We obtained the transcriptomic profiles of 952 tumors from 3 tumor types in TCGA with the highest frequency of MSI tumors (colorectal cancer, gastric cancer and endometrial cancer, **Figure 1**). As Epstein–Barr virus (EBV)-positive gastric tumors are also enriched for ICT responders[18,23], we grouped MSI and EBV tumors together as the responder-enriched group for gastric cancer. In total, the discovery cohort comprised of 1,486 tumors from 5 cancer types.

Tumor transcriptome deconvolution to identify features of ICT response in cancer and stromal cells

We performed tumor transcriptome deconvolution to estimate the stromal- and cancer-cell expression of each gene in tumors from responders (MSI) and non-responders (MSS) (**Figure 1**). Briefly, we first used a consensus-approach to infer tumor purities based on transcriptomic and genomic data (where available, Methods). For each ICT response group, we estimated gene expression levels in stromal and cancer cells using a non-negative least squares regression approach[17,24]. Finally, we identified cancer/stromal-cell differentially expressed genes (DEGs) between ICT responders and non-responders using a permutation-based statistic (**Figure 1, Supplementary Figure 1**).

118

119 **Top stromal genes associated with ICT response are enriched in immune pathways**

120 From this unbiased transcriptome-wide analysis, we identified 59 genes with differential
121 expression in stromal cells across all cohorts and tumor types (**Figure 2A-B, Supplementary**
122 **Figure 2A & C, Methods**). Among these DEGs, 51 (86%) had immune-related functions as
123 defined by the Gene Ontology (GO; see Methods), significantly higher than random
124 expectation (p < 2.2e-16, Fisher's Exact test). Stromal DEGs include genes involved in:
125 immune checkpoint signaling (e.g. *CD274*, *LAG3*, *CTLA4*), interferon gamma signaling (e.g.
126 *IFNG*, *IRF1*, *STAT1*), T-cell effector function (e.g. *PRF1*, *GZMA*, GZMB), and NK-cell mediated
127 cytotoxicity (*KLRD1*, *KLRC2*). Next, we performed pathway analysis to quantify the
128 enrichment of specific biological functions among the stromal DEGs associated with ICT
129 response. We identified 31 enriched GO biological process terms, all of which were immune
130 related (**Figure 2C**). These 31 terms could be further grouped into 4 clusters based on
131 similarity (see Methods): T cell activation, chemokine signaling, interferon-gamma response,
132 and natural killer cell mediated cytotoxicity **(Figure 2D**).

133 The top-2 DEGs with the greatest overexpression in ICT responders were chemokines
134 *CXCL9* and *CXCL13*. *CXCL9* is responsible for T-cell trafficking through binding the *CXCR3*
135 receptor on T-cells and has been associated with increased T-cell infiltration in tumors[25].
136 *CXCL13* is involved in both B-cell and T-cell migration via binding to the *CXCR5* receptor.
137 Production of *CXCL13* by T follicular helper cells (T_{FH}) is essential for tertiary lymphoid
138 structure formation at tumor sites as well as germinal center B cell activation[26], which has
139 been linked with anti-tumoral response to ICT[27]. Consistent with our meta-analysis, recent
140 studies have also proposed *CXCL9* and *CXCL13* as key predictors of improved ICT
141 response[28,29]. Remarkably, these two chemokines were also highlighted by a recent meta-

142 analysis that evaluated existing biomarkers of ICT response[30], suggesting that *CXCL9* and
143 *CXCL13* are indeed the strongest individual transcriptomic predictors of ICT response
144 independent of tumor type.
145
146 **Stromal genes negatively associated with ICT response**
147 Although high immune infiltration is generally associated with better ICT response[11,31,32],
148 our analysis uncovered a group of immune-related genes consistently associated with poor
149 ICT outcomes across tumor types. Among these genes, *FCER1A* showed the strongest and
150 most consistent overexpression in ICT non-responders. *FCER1A* encodes a subunit of the IgE
151 receptor. While *FCER1A* is an established marker of basophils, mast cells and dendritic cells,
152 it is also expressed on immunosuppressive M2 macrophages[33] and tumor associated
153 macrophages (TAMs)[34]. *CH25H*, a gene encoding enzyme cholesterol 25-hydroxylase that
154 catalyzes the formation of 25-hydroxycholesterol (25-HC), was also up-regulated in tumors
155 of ICT non-responders. Interestingly, 25-HC is produced by macrophages in response to
156 type-I interferon signalling and has numerous immunological effects including B-cell
157 chemotaxis, macrophage differentiation, and regulation of inflammatory response[35]. We
158 also observed two natriuretic peptides, NPR1 and NPR3, among genes up-regulated in ICT
159 non-responders. Although natriuretic peptides function primarily to regulate electrolytes,
160 they are expressed in immune cells and there is increasing evidence of their role in
161 inflammation and immunity[36].
162
163 **Immune cell subtype analysis identifies M1 macrophages as strong correlate of ICT**
164 **response**

165 To identify immune cell populations associated with ICT response, we estimated the
166 immune cell composition of each tumor using Cibersortx[37] and compared the abundance of
167 immune cell subsets between ICT responders and non-responders. M1 macrophages, T-
168 follicular helper (Tfh), and activated CD4 memory T-cells had higher abundance in ICT
169 responders as compared to non-responders (**Figure 3A, Supplementary Figure 3**). M1
170 macrophages are known to be pro-inflammatory and anti-tumoral[38]. A recent study found
171 M1 macrophage infiltration to be predictive to ICT response in urothelial cancer[39]. Our
172 results further demonstrate that M1 macrophage infiltration could be a general feature of
173 ICT response across multiple cancer types. Tfh cells are specialized CD4+ T cells that aid the
174 formation of germinal centers in tertiary lymphoid structures (TLS)[40], interacting with B-cells
175 to activate antibody responses[41] and enhancing CD8+ T-cell effector functions[42]. While the
176 presence of Tfh cells has been associated with favorable survival in multiple cancer
177 types[27,41-43], their putative role in ICT response has not been studied. Our analysis also
178 demonstrated that while resting CD4 memory T-cells were enriched in non-responders,
179 activated CD4 memory T-cells were enriched in ICT responders. This suggests that pre-
180 existing CD4+ T-cell immunity is important for effective anti-tumoral response upon ICT
181 treatment.

182 Next, we examined associations between the top DEGs and infiltration of specific
183 immune cell subsets. We found that the top gene expression markers of good ICT response
184 were generally associated with abundance of M1 macrophages, CD4+/CD8+ T-lymphocytes,
185 and activated NK cells (**Figure 3B, Supplementary Figure 4**). Using orthogonal expression
186 data of immune cells subtypes from flow cytometry and single-cell RNA-seq experiments,
187 we confirmed that *CXCL9* expression was strongly associated with M1 macrophage
188 infiltration, while *CXCL13* and *IFNG* expression were strongly associated with T-cell

189 infiltration (**Supplementary Figure 5**). Interestingly, the DEGs associated with poor ICT
190 response, including FCER1A, were correlated with resting state of mast cells, CD4+ memory
191 T cells, and dendritic cells, suggesting that these genes are likely markers of a quiescent or
192 immune-suppressive microenvironment (**Figure 3B, Supplementary Figure 4**).
193

194 **Cancer intrinsic features of ICT response tend to be tumor type specific**

195 Previous studies have proposed multiple mechanisms by which cancer cells may directly
196 suppress tumor immunity and impede ICT therapy[14,44]. Surprisingly, our meta-analysis
197 across tumor types revealed a paucity of DEGs associated with ICT response in cancer cells.
198 In cancer cells, we identified 9 genes differentially expressed between ICT responders and
199 ICT non-responders across tumor types (**Figure 4A, Supplementary Figure 2B & D**). In
200 addition, we observed that the differential expression signal for these 9 genes was mostly
201 driven by the MSI ICT-responder-enriched cohorts. As compared to stromal DEGs (**Figure**
202 **2A**), the signal for the cancer DEGs was less consistent across the distinct ICT cohorts (**Figure**
203 **4A**). Therefore, we hypothesize that the cancer DEGs identified by the meta-analysis are
204 likely related to biology of MSI tumors, rather than general mechanisms of ICT response. We
205 also confirmed that the paucity of cancer cell DEGs, as compared to stroma cell DEGs,
206 persisted regardless of the significance cutoff in our meta-analysis (**Figure 4B**), and we were
207 not able to identify functional enrichment or relationships among cancer DEGs.

208 Next, we conducted the same DEG analysis within individual tumor types to explore
209 the potential for tissue-dependent processes involved in ICT response. For melanoma, we
210 only identified 22 cancer DEGs shared between the 2 melanoma cohorts, and these genes
211 were not enriched in specific pathways. In gastric cancer, we identified 190 cancer ICT
212 response DEGs across the gastric ICT cohort and TCGA cohort. Interestingly, genes

213 associated with poor ICT response were enriched for angiogenesis-related functions (**Figure**
214 **4C**), with pro-angiogenic genes ENG, F2R and PDGFRB overexpressed in ICT non-responders
215 (MSI/EBV) compared to responders (MSS) (**Figure 4D**). These data are consistent with the
216 understanding that angiogenesis can be associated with immune suppression[45], suggesting
217 that a pro-angiogenic environment may impede ICT response in gastric cancer. In urothelial
218 cancer we found that cancer DEGs were enriched for neuron-related functional terms
219 (**Figure 4E**), with neuronal genes overexpressed in ICT responders compared to ICT non-
220 responders (**Figure 4F**). This observation is concordant with a previous study linking the
221 neuronal expression subtype[46] of urothelial cancer with poor overall survival but high
222 response rate to ICT[47].

223 Overall, while these results indicate an overall paucity of tissue-agnostic cancer-cell-
224 intrinsic features of ICT response, they also highlight the potential for tissue and tumor-type
225 specific expression signatures in cancer cells that may predict ICT response.

226

227 **Lack of cancer intrinsic immune checkpoint regulation across cancer types**

228 To further investigate if specific ligand-receptor interactions between cancer and immune
229 cells may promote primary ICT resistance, we systematically investigated the expression of
230 30 known immune checkpoint ligand-receptor pairs in both the cancer and stromal
231 components of the TME (**Figure 5A**). We found stromal overexpression of 13 checkpoint
232 receptors and 2 checkpoint ligands to be associated with ICT response across cancer types.
233 Checkpoint ligands PD-L1 and PD-L2 and their receptor PD-1 were coordinately upregulated
234 in the stroma of ICT responders compared to ICT non-responders. PD-L1 (*CD274*) and PD-1
235 were significantly upregulated in the stroma of ICT responders in 6 out of 7 cohorts studied
236 (p-value<0.05, permutation test), while PD-L2 was upregulated in 5 out of the 7 cohorts

237 (**Supplementary Figure 6).** Interestingly, no checkpoint ligands were consistently
238 differentially expressed and associated with ICT response in cancer cells across tumor types.
239 In addition to immune checkpoints, cytokines also play important roles in tumor
240 immunity[48-50]. We examined the expression of 13 pairs of cytokines and cytokine receptors
241 known to be involved in tumor immunity[48,50], aiming to identify cytokine signals associated
242 with ICT response (**Figure 5B**). Similar to our analysis for immune checkpoints, we found
243 that cancer-intrinsic cytokine expression was not associated with ICT response across tumor
244 types. However, six cytokines (*IFNG*, *FASLG*, *CXCL13*, *CCL5*, *CXCL10* and *CXCL9*), and the
245 corresponding receptors for three of the cytokines (*CCR5* for *CCL5*, *CXCR3* for *CXCL9* and
246 *CXCL10*) were significantly upregulated in the stroma of ICT responders, consistent with
247 previous observations[11,21]. Overall, our analysis finds no evidence for a universal mechanism
248 by which cancer cells inhibit immune cells via checkpoints interactions or
249 chemokine/cytokine signaling.
250
251 **A 3-feature classifier robustly predicts ICT response across cancer types**
252 Next, we explored if we could build an accurate predictor of ICT response based on the
253 consensus DEGs identified earlier (**Figure 6A**). We focused on the 59 stroma-specific DEGs
254 (**Figure 2A**) as they were more consistent across tumor types, in comparison to cancer DEGs,
255 and therefore more likely to be generalize to unseen cancer types. While a stroma
256 transcriptomic signature would likely reflect the state and favorability of the tumor
257 microenvironment for ICT response, TMB is likely a proxy of the tumor immunogenicity.
258 Since the stroma DEGs and TMB likely represent different facets of tumor immunity, we
259 hypothesized that these could be orthogonal predictors of ICT response and therefore
260 considered both factors for the predictive model. To identify the best predictive features of

261 ICT response, we used LASSO logistic regression with 10-fold cross-validation to select
262 robust features from the set of 59 stromal DEGs and TMB (**Figure 6A**). The final model was
263 built using the top-3 features: TMB, *IFNG* expression, and *FCER1A* expression (**Figure 6B**).
264 The model was trained on 461 samples from the ICT discovery cohorts with both
265 transcriptomic and genomic data. Next, we evaluated the model performance on 2
266 independent test cohorts. Test cohort 1 consisted of 49 tumors from melanoma patients
267 treated with the PD-L1 inhibitor nivolumab[51]. Test cohort 2 consisted of 87 tumors from 20
268 solid cancer types treated with a mix of ICT agents[52]. We calculated the areas under the
269 receiver operating curve (AUC) of our model, and benchmarked it against published
270 biomarkers of ICT response, namely CXCL9+TMB[30], T-cell GEP[11], TIDE[13,53], TMB alone[2,8], and
271 PD-L1 expression[3]. Intriguingly, our 3-feature predictor outperformed all existing biomarkers.
272 On test cohort 1, the 3-feature model achieved an AUC of 0.66, compared to 0.62 for
273 CXCL9+TMB, 0.64 for T-cell GEP, 0.44 for TIDE, 0.55 for PD-L1 expression, and 0.57 for the
274 TMB-only model. On test cohort 2, the model achieved an AUC of 0.72, compared to 0.67
275 for CXCL9+TMB, 0.63 for T-cell GEP, 0.32 for TIDE, 0.61 for PD-L1 expression, and 0.55 for
276 the TMB-only model (**Figure 6C**). This demonstrates that *FCER1A,* a novel negative
277 biomarker of ICT response identified from our transcriptome-wide analysis, contribute
278 additional predictive power of ICT response over existing biomarkers.
279

280 **Discussion**

281 In this study, we performed a transcriptome-wide meta-analysis of ICT response in 1486
282 tumors. These tumor samples included 534 tumors with annotated clinical response to ICT
283 treatment, and 952 tumors from cancer types enriched for MSI and ICT-responding tumors.
284 Using *in silico* tumor transcriptome deconvolution, we analyzed gene expression signatures

285 of cancer and stromal cells and identified differentially expressed genes (DEGs) associated
286 with ICT response across tumor types. Strikingly, this meta-analysis revealed a paucity of
287 ICT-response DEGs in cancer cells as compared to stromal cells. The few cancer DEGs that
288 we identified by the meta-analysis were more likely related to the biology of MSI tumors
289 and their DNA mismatch repair deficiency rather than being general determinants of ICT
290 response. In contrast, our analysis revealed 59 stroma-specific ICT-response DEGs, which
291 were strongly enriched in immune-related pathways and processes (**Figure 7**).

292 The two chemokine ligands, *CXCL9* and *CXCL13*, constituted the top-2 stromal genes
293 overexpressed in ICT responders. Underlining the validity of our approach, these two genes
294 have been highlighted for their roles in anti-tumor immunity and association with favorable
295 ICT response in multiple recent studies[28-30]. Previous studies suggest CXCL13 may play dual
296 roles in ICT response. First, CXCL13 is produced by Tfh cells and involved in B-cell
297 organization in TLS [26], and the presence of TLS can be a positive predictor of ICT
298 response[27,42]. Second, *CXCL13* has been reported to be highly expressed by neo-antigen
299 reactive CD8+ T-cells directly involved in cancer cell killing [54,55]. In line with these findings,
300 we found enrichment of both Tfh and CD8+ T-cells in tumors of ICT responders compared to
301 non-responders across cancer types (**Figure 3,7**). Additionally, the abundance of these two
302 cell types correlates with *CXCL13* expression. In agreement with recent work, we found that
303 *CXCL9* expression is strongly correlated with M1 macrophage infiltration[28,56], and M1
304 macrophages were one of the most differentially enriched immune cell types in ICT
305 responders (**Figure 3a**). Although myeloid infiltration has traditionally been associated with
306 immune suppression[38], our data is consistent with the hypothesis that M1 macrophage
307 infiltration, and macrophage polarization, could be an important determinant of tumor
308 sensitivity to ICT.

309 Intriguingly, we also identified a set of immune-related genes that were negatively
310 associated with ICT response. Among these genes, *FCER1A* and *CH25H* have previously been
311 reported to be over-expressed in anti-inflammatory M2 macrophages[33,57], and FCER1A+
312 TAMs have been reported to promote tumor progression by engaging in a positive feedback
313 loop with tumor initiating cells[34].

314 Interestingly, we observed an enrichment of the resting states of CD4 memory T-
315 cells, dendritic cells and mast cells in ICT non-responders. In contrast, the activated states of
316 these cell types are enriched in the tumors of ICT responders (**Figure 3B**). Furthermore,
317 while *FCER1A* is expressed in antigen presenting cells like dendritic cells and macrophages,
318 we noted that its expression is 25 times higher in resting dendritic cells compared to
319 activated dendritic cells, and 14 times higher in M2 macrophages compared to M1
320 macrophages[37]. These results suggest that a pre-existing immunosuppressive
321 microenvironment, associated with resting immune cells and high *FCER1A* expression, may
322 prevent effective anti-tumor immune responses in ICT non-responders.

323 Analyses of immune checkpoint and cytokine ligand-receptor interactions revealed
324 coordinated upregulation of several ligand-receptor pairs in the stroma of tumors from ICT
325 responders, including genes encoding PD-L1/PD-L2 and their receptor PD-1, CXCL9/CXCL10
326 and their receptor CXCR3, and CCL5 and its receptor CCR5 (**Figure 5, Figure 7**). In contrast,
327 we did not find consistent expression changes of checkpoint proteins and cytokines in
328 cancer cells of ICT responders. Currently, PD-L1 expression on both cancer cells and
329 infiltrating immune cells are used as biomarkers to stratify patients for ICT[14]. Our study
330 provides evidence that PD-L1 expression on immune cells could be a more consistent
331 determinant of ICT response across tumor types. Among chemokines upregulated in ICT
332 responders, CXCL9, CXCL10, and CXCL13 promote lymphocyte recruitment, while CCL5 is a

333 chemoattractant of myeloid cells. CCL5 recruits CCR5+ blood monocytes and neutrophils
334 that can differentiate into immunosuppressive tumor associated macrophages and
335 neutrophils[48,49]. In addition, CCL5 also has direct pro-tumoral effects on cancer cells,
336 promoting cancer proliferation and metastasis[48,49]. Preclinical and clinical studies suggested
337 that targeting the CCL5-CCR5 axis could enhance anti-tumoral response[58,59]. As *CCL5* and
338 *CCR5* are both overexpressed in ICT responders, our result suggests that targeting CCL5-
339 CCR5 signaling in conjunction with ICT might further potentiate anti-tumoral immune
340 response.

341 Using the stromal consensus DEGs identified from the meta-analysis, we developed
342 a model to predict ICT response from gene expression data and TMB. This 3-feature model
343 comprised of a single positive marker of immune infiltration (*IFNG*), a single negative marker
344 of immune suppression (*FCER1A*), in combination with TMB. The model robustly predicted
345 ICT response across both the discovery cohort and 2 independent test cohorts,
346 outperforming existing gene expression signatures for ICT response. While ideal pan-cancer
347 biomarkers of ICT response should be robust across patient cohorts, we noticed that the Liu
348 et al. melanoma cohort did not share many DEGs with the other cohorts, including other
349 melanoma cohorts. This result highlights significant heterogeneity between ICT cohorts,
350 even among cohorts of the same tumor type. It is unclear to what extent this heterogeneity
351 arise from patient selection, differences in ICT regime, differences in prior treatments,
352 different sample collection protocols, or differences in gene expression assays. This
353 highlights the need for large, consistently selected patient cohorts, with standardized gene
354 expression profiling to further improve biomarker discovery.

355 As cancer cells are under negative selective pressure from the immune system,
356 several mechanisms of immune escape by cancer cells have been proposed: (i) cancer cells

357 down-regulate antigen presentation by deleting HLA alleles[44], (ii) cancer cells deplete
358 neoantigens to avoid detection[60], (iii) oncogenic signaling may up-regulate PD-L1 expression
359 and suppress T-cell recruitment[61]. However, the prevalence of these immune evasion
360 mechanisms are still unclear. A recent meta-analysis found no association between loss of
361 heterozygosity of HLA alleles and ICT response across ICT cohorts[30]. Furthermore, a pan-
362 cancer analysis failed to detect neo-antigen depletion signals in most tumor types[62].
363 Similarly, we found a lack of conserved cancer-intrinsic mechanisms of immune evasion on
364 the transcriptomic level. These results suggest that cancer cells adopt diverse mechanisms
365 of immune evasion, with no universal strategy adopted by cancer cells to avoid immune-
366 mediated killing. The growing number of molecularly characterized ICT cohorts will enable
367 further exploration of the importance and prevalence of the different cancer-intrinsic
368 immune evasion strategies in determining ICT response.
369
370

371 **Methods**

372 **Clinical cohorts treated with ICT**

373 Data from the following studies were used for discovery:

374 1. Kim et al.[18] cohort comprises of 45 metastatic gastric cancer patients treated with
375 PD-1 inhibitor pembrolizumab
376 2. Mariathasan et al.[19] cohort comprises of 298 metastatic urothelial cancer patients
377 treated with PD-L1 inhibitor atezolizumab
378 3. Liu et al. [21] comprises of 118 metastatic melanoma patients treated with PD-1
379 inhibitors nivolumab or pembrolizumab
380 4. Gide et al. [20] comprises of 73 metastatic melanoma patients treated with anti-PD-1
381 alone (nivolumab or pembrolizumab, or with anti-CTLA-4 (nivolumab or
382 pembrolizumab with ipilimumab)

383 Data from the following studies were used for validation:

384 1. Riaz et al. [51] comprises 49 advanced melanoma patients treated with PD-L1 inhibitor
385 nivolumab.
386 2. Pender et al.[52] comprises of 87 metastatic tumors from 20 solid cancer types treated
387 with a mix of ICT agents.

388

389 **Gene expression data collection and normalization**

390 Expression data of TCGA colorectal (COAD, READ), gastric (STAD) and endometrial (UCEC)
391 tumors were downloaded from the UCSC Xena repository. Raw genomic and transcriptomic
392 data of Kim et al.[18] gastric ICT cohort were downloaded from the European Nucleotide
393 Archive, and processed using the bcbio nextgen pipeline. Briefly, RNAseq reads were aligned
394 to the human transcriptome using STAR[63], and TPM counts were quantified using SALMON[64].

395 Processed transcriptomic data of Mariathasan et al. (urothelial)[19], Liu et al. (melanoma)[21],
396 Gide et al. (melanoma)[20], Riaz et al. (melanoma)[51], and Pender et al. (mixed)[52] ICT cohorts
397 were obtained from the original publications. Genes with 0 expression in more than 50% of
398 the samples were removed. All gene expression data were log2 transformed and upper
399 quantile normalized across all cohorts.
400

401 **Tumor purity estimation**

402 Purity estimates of TCGA tumors were obtained from a previous publication[17], where
403 consensus purity was estimated from mutation allele frequencies, copy number variations
404 and RNA profiles of each tumor. Tumor purity of samples from ICT cohorts were estimated
405 using PUREE[65], a machine learning method for tumor purity estimation from bulk RNA
406 transcriptomics. For the Kim et al. gastric ICT cohort[47] where genomic data is also available,
407 we calculated consensus purity estimates based on both genomic and transcriptomic data.
408 We first computed purity estimates using 2 RNA-based methods (PUREE[65] and Estimate[66]),
409 and 2 DNA-based methods (Sequenza[67], PurBayes[68]). Then, we performed quantile-quantile
410 normalization on the purity estimates of individual methods, and took the mean normalized
411 purity estimate as the consensus purity.
412

413 **MSI status and ICT response classification**

414 MSI status of TCGA tumors were obtained from two previous pan-cancer studies of
415 microsatellite instability[9,10]. EBV status of the TCGA STAD tumors was obtained from a
416 previous TCGA study on gastrointestinal cancers[69].Clinical annotations of ICT response
417 based on the RECIST criteria were obtained from the original studies. Consistent with recent
418 literature[19,30], we classified "CR/PR" as responders and "SD/PD" as non-responders.

419

420 **Expression deconvolution**

421 We modelled bulk tumor expression as the sum of cancer and stroma expression, weighted

422 by cancer purity[17]. This can be written as,

423

$$y_j = c_j p + s_j(1 - p) + \varepsilon_j$$

424 where y_j is a *n* x 1 vector of bulk tumor expression for gene *j* in *n* samples, c_j and s_j are the

425 average cancer- and stroma-specific expression for a gene *j*, p is *n* x 1 vector of cancer purity,

426 and ε_j is the residual. Given bulk expression (y_j) and tumor purity (p), non-negative least

427 squares (NNLS) regression can be used to estimate cancer- (c_j) and stroma-specific (s_j)

428 expression for each gene. c_j and s_j represent estimates of mean cancer- and stroma-specific

429 expression for a gene j for $p_c = 1$ and $p_s = 0$, respectively. The standard error of these

430 predicted values for gene *j* is calculated as,

431

$$SE_{j,h} = \sqrt{MSE + \left(1 + \frac{1}{n} + \frac{(p_h - \bar{p})^2}{\sum(p_i - \bar{p})^2}\right)}$$

432

433 where $p_h = p_c = 1$ for cancer-specific expression and $p_h = p_s = 0$ for stroma-specific

434 expression; MSE is the mean square error.

435

436 **Permutation statistic to identify differentially expressed genes**

437 To test differences in cancer (or stroma) expression between two response groups (e.g.

438 $c_{Rj} - c_{NRj}$ for gene *j*), the above approach is applied to each group separately, and a test

439 statistic is calculated as,

440

$$Z_{obs,j}^2 = \left(\frac{c_{Rj} - c_{NRj}}{\sqrt{SE_{Rj}^2 + SE_{NRj}^2}} \right)^2$$

441

442 To assess significance under the null hypothesis of no difference in cancer (stroma)
443 expression between the 2 response groups, a null distribution is generated by permutation,
444 where group labels are first randomly shuffled 10,000 times and the above procedure is
445 applied to each permuted dataset, generating a null distribution of Z_{perm}^2 statistics. A p-
446 value is calculated as,

447

$$p = P\left(Z_{perm}^2 \geq Z_{obs}^2\right)$$

448

449 That is, the probability of observing Z_{obs}^2 or larger, given the null hypothesis is true.

450

451 **Identification of consensus DEGs across cancer types**

452 For each gene and each tumor compartment (caner or stroma), a meta p-value is computed
453 by combining the permutation p-values of all cancer cohorts using Fisher's method. We
454 used the Bonferroni correction to adjust for multiple testing to maintain the overall α at
455 0.01. Genes that are differentially expressed in different directions in at least 2 cohorts were
456 removed. Finally, to eliminate DEGs that are involved in MSI biology but are not directly
457 associated with ICT response, we require the final list of consensus DEGs to be differentially
458 expressed in at least 1 ICT cohort (nominal p-value<0.1).

459

460 **Pathway enrichment analysis**

461 To find out if the DEGs identified are enriched in specific biological processes, pathway
462 enrichment analysis was performed using ClueGo[70] with default parameters. Briefly, two-
463 sided-hypergeometric statistic was used to compute the enrichment of a given list of DEGs
464 in GO biological processes terms, and the resulting p-values were corrected for multiple
465 testing using the Bonferroni step down approach. To aid interpretation, significant biological
466 terms with high overlap as measured by the kappa coefficient were merged into functional
467 groups. To calculate the enrichment of stroma DEGs in immune-related functions, we
468 defined immune-related genes as genes in the "immune system process" term and its child
469 terms in the GO biological processes dataset. Additionally, we manually curated stroma
470 DEGs not labeled as immune genes by GO, and further labeled *FCER1A*, *GZMH*, *FCRL6*, *SIRPG*,
471 *JAKMIP1*, and *WARS* as immune-related genes based on literature search.

472

473 **Building a predictive model of ICT response**

474 We used 461 patients from 3 discover cohorts (Mariathasan et al[19], Liu et al[21], Kim et al.[18])
475 with both transcriptomic data and TMB as training data. TMB was obtained from the
476 original publications and standardized into Z-scores (mean=0, standard deviation=1). To
477 identify the most predictive features of ICT response, we used the least absolute shrinkage
478 and selection operator (LASSO) to select features from the 59 stroma DEGs identified earlier
479 and TMB. LASSO penalizes the sum of the absolute values of the regression coefficients,
480 shrinking some coefficients to zero, and thereby identifies a simpler and more interpretable
481 model. The regularization parameter λ was chosen by 10-fold cross-validation such that the
482 error of the selected model was within 1 standard deviation from the minimum error.
483 LASSO regression and cross validation were performed using the 'glmnet' package in R. To

484 select for the most robust features, we bootstrapped 100 samples with 90% of the data in
485 each bootstrap, and selected features that are found by at least 75% of the bootstraps for
486 the final model. The final logistic regression model is built on all 461 training samples using
487 the features selected by LASSO (TMB+IFNG+FCER1A).
488
489 **Benchmarking ICT prediction model against existing biomarkers**
490 T-cell GEP scores were calculated from normalized RNAseq data using the weights provided
491 by Ayers et al. 2018[11]. TIDE scores were calculated from normalized RNAseq data using the
492 TIDE web platform[53]. The CXCL-9+TMB model was trained on our training cohort using
493 logistic regression.
494
495 **Immune cell enrichment analysis**
496 Immune deconvolution was performed using CibersortX (with the LM22 signature matrix)[37]
497 to estimate the absolute abundance of immune cell subsets for each tumor. Immune cell
498 subsets that are differentially infiltrated between responders and non-responders were
499 identified using the Wilcoxon rank-sum test.
500
501 **Data and code availability**
502 The code used to generate figures in the manuscript is provided in **Supplementary Data 1**.
503
504 **Acknowledgements**
505 This study was supported by the Singapore Ministry of Health's National Medical Research
506 Council under its OF-IRG program (OFIRG18may-0075) and Singapore Agency for Science,

Technology and Research (A*STAR) under its Biomedical Engineering Programme (C221118001 and C221318004)

509 **References**

510 1. O'Reilly EM, Oh DY, Dhani N, et al. Durvalumab With or Without Tremelimumab for
511 Patients With Metastatic Pancreatic Ductal Adenocarcinoma: A Phase 2 Randomized Clinical
512 Trial. *JAMA Oncol*. Oct 1 2019;5(10):1431-1438. doi:10.1001/jamaoncol.2019.1588
513 2. Yarchoan M, Hopkins A, Jaffee EM. Tumor Mutational Burden and Response Rate to
514 PD-1 Inhibition. *N Engl J Med*. 12 21 2017;377(25):2500-2501. doi:10.1056/NEJMc1713444
515 3. Havel JJ, Chowell D, Chan TA. The evolving landscape of biomarkers for checkpoint
516 inhibitor immunotherapy. *Nat Rev Cancer*. 03 2019;19(3):133-150. doi:10.1038/s41568-019-
517 0116-x
518 4. Marcus L, Lemery SJ, Keegan P, Pazdur R. FDA Approval Summary: Pembrolizumab
519 for the Treatment of Microsatellite Instability-High Solid Tumors. *Clin Cancer Res*. 07 01
520 2019;25(13):3753-3758. doi:10.1158/1078-0432.CCR-18-4070
521 5. FDA approves pembrolizumab for adults and children with TMB-H solid tumors. June
522 17, 2020.
523 6. Banchereau R, Leng N, Zill O, et al. Molecular determinants of response to PD-L1
524 blockade across tumor types. *Nat Commun*. 06 25 2021;12(1):3969. doi:10.1038/s41467-
525 021-24112-w
526 7. Valero C, Lee M, Hoen D, et al. Response Rates to Anti-PD-1 Immunotherapy in
527 Microsatellite-Stable Solid Tumors With 10 or More Mutations per Megabase. *JAMA Oncol*.
528 May 01 2021;7(5):739-743. doi:10.1001/jamaoncol.2020.7684
529 8. Samstein RM, Lee CH, Shoushtari AN, et al. Tumor mutational load predicts survival
530 after immunotherapy across multiple cancer types. *Nat Genet*. 02 2019;51(2):202-206.
531 doi:10.1038/s41588-018-0312-8
532 9. Cortes-Ciriano I, Lee S, Park WY, Kim TM, Park PJ. A molecular portrait of
533 microsatellite instability across multiple cancers. *Nat Commun*. 06 06 2017;8:15180.
534 doi:10.1038/ncomms15180
535 10. Bonneville R, Krook MA, Kautto EA, et al. Landscape of Microsatellite Instability
536 Across 39 Cancer Types. *JCO Precis Oncol*. 2017;2017doi:10.1200/PO.17.00073
537 11. Ayers M, Lunceford J, Nebozhyn M, et al. IFN-γ-related mRNA profile predicts clinical
538 response to PD-1 blockade. *J Clin Invest*. Aug 01 2017;127(8):2930-2940.
539 doi:10.1172/JCI91190
540 12. Cristescu R, Mogg R, Ayers M, et al. Pan-tumor genomic biomarkers for PD-1
541 checkpoint blockade-based immunotherapy. *Science*. Oct 12
542 2018;362(6411)doi:10.1126/science.aar3593
543 13. Jiang P, Gu S, Pan D, et al. Signatures of T cell dysfunction and exclusion predict
544 cancer immunotherapy response. *Nat Med*. 10 2018;24(10):1550-1558.
545 doi:10.1038/s41591-018-0136-1
546 14. Nishino M, Ramaiya NH, Hatabu H, Hodi FS. Monitoring immune-checkpoint
547 blockade: response evaluation and biomarker development. *Nat Rev Clin Oncol*. Nov
548 2017;14(11):655-668. doi:10.1038/nrclinonc.2017.88
549 15. Guruprasad P, Lee YG, Kim KH, Ruella M. The current landscape of single-cell
550 transcriptomics for cancer immunotherapy. *J Exp Med*. Jan 4
551 2021;218(1)doi:10.1084/jem.20201574
552 16. Gohil SH, Iorgulescu JB, Braun DA, Keskin DB, Livak KJ. Applying high-dimensional
553 single-cell technologies to the analysis of cancer immunotherapy. *Nat Rev Clin Oncol*. Apr
554 2021;18(4):244-256. doi:10.1038/s41571-020-00449-x

555 17. Ghoshdastider U, Rohatgi N, Mojtabavi Naeini M, et al. Pan-Cancer Analysis of
556 Ligand-Receptor Cross-talk in the Tumor Microenvironment. *Cancer Res*. 04 01
557 2021;81(7):1802-1812. doi:10.1158/0008-5472.CAN-20-2352
558 18. Kim ST, Cristescu R, Bass AJ, et al. Comprehensive molecular characterization of
559 clinical responses to PD-1 inhibition in metastatic gastric cancer. *Nat Med*. 09
560 2018;24(9):1449-1458. doi:10.1038/s41591-018-0101-z
561 19. Mariathasan S, Turley SJ, Nickles D, et al. TGFβ attenuates tumour response to PD-L1
562 blockade by contributing to exclusion of T cells. *Nature*. 02 22 2018;554(7693):544-548.
563 doi:10.1038/nature25501
564 20. Gide TN, Quek C, Menzies AM, et al. Distinct Immune Cell Populations Define
565 Response to Anti-PD-1 Monotherapy and Anti-PD-1/Anti-CTLA-4 Combined Therapy. *Cancer*
566 *Cell*. 02 11 2019;35(2):238-255.e6. doi:10.1016/j.ccell.2019.01.003
567 21. Liu D, Schilling B, Sucker A, et al. Integrative molecular and clinical modeling of
568 clinical outcomes to PD1 blockade in patients with metastatic melanoma. *Nat Med*. 12
569 2019;25(12):1916-1927. doi:10.1038/s41591-019-0654-5
570 22. Green AK, Feinberg J, Makker V. A Review of Immune Checkpoint Blockade Therapy
571 in Endometrial Cancer. *Am Soc Clin Oncol Educ Book*. Mar 2020;40:1-7.
572 doi:10.1200/EDBK_280503
573 23. Kubota Y, Kawazoe A, Sasaki A, et al. The Impact of Molecular Subtype on Efficacy of
574 Chemotherapy and Checkpoint Inhibition in Advanced Gastric Cancer. *Clin Cancer Res*. 07 15
575 2020;26(14):3784-3790. doi:10.1158/1078-0432.CCR-20-0075
576 24. Rohatgi N, Ghoshdastider U, Baruah P, Kulshrestha T, Skanderup AJ. A pan-cancer
577 metabolic atlas of the tumor microenvironment. *Cell Rep*. May 10 2022;39(6):110800.
578 doi:10.1016/j.celrep.2022.110800
579 25. Gorbachev AV, Kobayashi H, Kudo D, et al. CXC chemokine ligand 9/monokine
580 induced by IFN-gamma production by tumor cells is critical for T cell-mediated suppression
581 of cutaneous tumors. *J Immunol*. Feb 15 2007;178(4):2278-86.
582 doi:10.4049/jimmunol.178.4.2278
583 26. Kazanietz MG, Durando M, Cooke M. CXCL13 and Its Receptor CXCR5 in Cancer:
584 Inflammation, Immune Response, and Beyond. *Front Endocrinol (Lausanne)*. 2019;10:471.
585 doi:10.3389/fendo.2019.00471
586 27. Hollern DP, Xu N, Thennavan A, et al. B Cells and T Follicular Helper Cells Mediate
587 Response to Checkpoint Inhibitors in High Mutation Burden Mouse Models of Breast Cancer.
588 *Cell*. 11 14 2019;179(5):1191-1206.e21. doi:10.1016/j.cell.2019.10.028
589 28. Qu Y, Wen J, Thomas G, et al. Baseline Frequency of Inflammatory Cxcl9-Expressing
590 Tumor-Associated Macrophages Predicts Response to Avelumab Treatment. *Cell Rep*. 07 07
591 2020;32(1):107873. doi:10.1016/j.celrep.2020.107873
592 29. Goswami S, Chen Y, Anandhan S, et al. mutation plus CXCL13 expression act as
593 combinatorial biomarkers to predict responses to immune checkpoint therapy in mUCC. *Sci*
594 *Transl Med*. 06 17 2020;12(548)doi:10.1126/scitranslmed.abc4220
595 30. Litchfield K, Reading JL, Puttick C, et al. Meta-analysis of tumor- and T cell-intrinsic
596 mechanisms of sensitization to checkpoint inhibition. *Cell*. 02 04 2021;184(3):596-614.e14.
597 doi:10.1016/j.cell.2021.01.002
598 31. Rooney MS, Shukla SA, Wu CJ, Getz G, Hacohen N. Molecular and genetic properties
599 of tumors associated with local immune cytolytic activity. *Cell*. Jan 15 2015;160(1-2):48-61.
600 doi:10.1016/j.cell.2014.12.033

601 32. Fehrenbacher L, Spira A, Ballinger M, et al. Atezolizumab versus docetaxel for
602 patients with previously treated non-small-cell lung cancer (POPLAR): a multicentre, open-
603 label, phase 2 randomised controlled trial. *Lancet*. Apr 30 2016;387(10030):1837-46.
604 doi:10.1016/S0140-6736(16)00587-0
605 33. Pellizzari G, Hoskin C, Crescioli S, et al. IgE re-programs alternatively-activated
606 human macrophages towards pro-inflammatory anti-tumoural states. *EBioMedicine*. May
607 2019;43:67-81. doi:10.1016/j.ebiom.2019.03.080
608 34. Taniguchi S, Elhance A, Van Duzer A, Kumar S, Leitenberger JJ, Oshimori N. Tumor-
609 initiating cells establish an IL-33-TGF-β niche signaling loop to promote cancer progression.
610 *Science*. 07 17 2020;369(6501)doi:10.1126/science.aay1813
611 35. Cyster JG, Dang EV, Reboldi A, Yi T. 25-Hydroxycholesterols in innate and adaptive
612 immunity. *Nat Rev Immunol*. Nov 2014;14(11):731-43. doi:10.1038/nri3755
613 36. Vollmar AM. The role of atrial natriuretic peptide in the immune system. *Peptides*.
614 Jun 2005;26(6):1086-94. doi:10.1016/j.peptides.2004.08.034
615 37. Newman AM, Steen CB, Liu CL, et al. Determining cell type abundance and
616 expression from bulk tissues with digital cytometry. *Nat Biotechnol*. 07 2019;37(7):773-782.
617 doi:10.1038/s41587-019-0114-2
618 38. Duan Z, Luo Y. Targeting macrophages in cancer immunotherapy. *Signal Transduct*
619 *Target Ther*. 03 26 2021;6(1):127. doi:10.1038/s41392-021-00506-6
620 39. Zeng D, Ye Z, Wu J, et al. Macrophage correlates with immunophenotype and
621 predicts anti-PD-L1 response of urothelial cancer. *Theranostics*. 2020;10(15):7002-7014.
622 doi:10.7150/thno.46176
623 40. Crotty S. T Follicular Helper Cell Biology: A Decade of Discovery and Diseases.
624 *Immunity*. 05 21 2019;50(5):1132-1148. doi:10.1016/j.immuni.2019.04.011
625 41. Garaud S, Buisseret L, Solinas C, et al. Tumor infiltrating B-cells signal functional
626 humoral immune responses in breast cancer. *JCI Insight*. 08 13
627 2019;5doi:10.1172/jci.insight.129641
628 42. Cui C, Wang J, Fagerberg E, et al. Neoantigen-driven B cell and CD4 T follicular helper
629 cell collaboration promotes anti-tumor CD8 T cell responses. *Cell*. 12 09 2021;184(25):6101-
630 6118.e13. doi:10.1016/j.cell.2021.11.007
631 43. Bindea G, Mlecnik B, Tosolini M, et al. Spatiotemporal dynamics of intratumoral
632 immune cells reveal the immune landscape in human cancer. *Immunity*. Oct 17
633 2013;39(4):782-95. doi:10.1016/j.immuni.2013.10.003
634 44. Kalbasi A, Ribas A. Tumour-intrinsic resistance to immune checkpoint blockade. *Nat*
635 *Rev Immunol*. Jan 2020;20(1):25-39. doi:10.1038/s41577-019-0218-4
636 45. Motz GT, Coukos G. The parallel lives of angiogenesis and immunosuppression:
637 cancer and other tales. *Nat Rev Immunol*. 09 23 2011;11(10):702-11. doi:10.1038/nri3064
638 46. Robertson AG, Kim J, Al-Ahmadie H, et al. Comprehensive Molecular
639 Characterization of Muscle-Invasive Bladder Cancer. *Cell*. 08 09 2018;174(4):1033.
640 doi:10.1016/j.cell.2018.07.036
641 47. Kim J, Kwiatkowski D, McConkey DJ, et al. The Cancer Genome Atlas Expression
642 Subtypes Stratify Response to Checkpoint Inhibition in Advanced Urothelial Cancer and
643 Identify a Subset of Patients with High Survival Probability. *Eur Urol*. 06 2019;75(6):961-964.
644 doi:10.1016/j.eururo.2019.02.017
645 48. Nagarsheth N, Wicha MS, Zou W. Chemokines in the cancer microenvironment and
646 their relevance in cancer immunotherapy. *Nat Rev Immunol*. Sep 2017;17(9):559-572.
647 doi:10.1038/nri.2017.49

648 49. Mollica Poeta V, Massara M, Capucetti A, Bonecchi R. Chemokines and Chemokine
649 Receptors: New Targets for Cancer Immunotherapy. *Front Immunol*. 2019;10:379.
650 doi:10.3389/fimmu.2019.00379
651 50. Dranoff G. Cytokines in cancer pathogenesis and cancer therapy. *Nat Rev Cancer*. Jan
652 2004;4(1):11-22. doi:10.1038/nrc1252
653 51. Riaz N, Havel JJ, Makarov V, et al. Tumor and Microenvironment Evolution during
654 Immunotherapy with Nivolumab. *Cell*. Nov 02 2017;171(4):934-949.e16.
655 doi:10.1016/j.cell.2017.09.028
656 52. Pender A, Titmuss E, Pleasance ED, et al. Genome and Transcriptome Biomarkers of
657 Response to Immune Checkpoint Inhibitors in Advanced Solid Tumors. *Clin Cancer Res*. 01
658 01 2021;27(1):202-212. doi:10.1158/1078-0432.CCR-20-1163
659 53. Fu J, Li K, Zhang W, et al. Large-scale public data reuse to model immunotherapy
660 response and resistance. *Genome Med*. Feb 26 2020;12(1):21. doi:10.1186/s13073-020-
661 0721-z
662 54. Zheng C, Fass JN, Shih YP, et al. Transcriptomic profiles of neoantigen-reactive T cells
663 in human gastrointestinal cancers. *Cancer Cell*. 04 11 2022;40(4):410-423.e7.
664 doi:10.1016/j.ccell.2022.03.005
665 55. Lowery FJ, Krishna S, Yossef R, et al. Molecular signatures of antitumor neoantigen-
666 reactive T cells from metastatic human cancers. *Science*. 02 25 2022;375(6583):877-884.
667 doi:10.1126/science.abl5447
668 56. House IG, Savas P, Lai J, et al. Macrophage-Derived CXCL9 and CXCL10 Are Required
669 for Antitumor Immune Responses Following Immune Checkpoint Blockade. *Clin Cancer Res*.
670 01 15 2020;26(2):487-504. doi:10.1158/1078-0432.CCR-19-1868
671 57. Preuss I, Ludwig MG, Baumgarten B, et al. Transcriptional regulation and functional
672 characterization of the oxysterol/EBI2 system in primary human macrophages. *Biochem*
673 *Biophys Res Commun*. Apr 11 2014;446(3):663-8. doi:10.1016/j.bbrc.2014.01.069
674 58. Halama N, Zoernig I, Berthel A, et al. Tumoral Immune Cell Exploitation in Colorectal
675 Cancer Metastases Can Be Targeted Effectively by Anti-CCR5 Therapy in Cancer Patients.
676 *Cancer Cell*. Apr 11 2016;29(4):587-601. doi:10.1016/j.ccell.2016.03.005
677 59. Ban Y, Mai J, Li X, et al. Targeting Autocrine CCL5-CCR5 Axis Reprograms
678 Immunosuppressive Myeloid Cells and Reinvigorates Antitumor Immunity. *Cancer Res*. 06 01
679 2017;77(11):2857-2868. doi:10.1158/0008-5472.CAN-16-2913
680 60. Zapata L, Caravagna G, Williams MJ, et al. Immune selection determines tumor
681 antigenicity and influences response to checkpoint inhibitors. *Nat Genet*. Mar
682 2023;55(3):451-460. doi:10.1038/s41588-023-01313-1
683 61. Spranger S, Gajewski TF. Impact of oncogenic pathways on evasion of antitumour
684 immune responses. *Nat Rev Cancer*. Mar 2018;18(3):139-147. doi:10.1038/nrc.2017.117
685 62. Van den Eynden J, Jimenez-Sanchez A, Miller ML, Larsson E. Lack of detectable
686 neoantigen depletion signals in the untreated cancer genome. *Nat Genet*. Dec
687 2019;51(12):1741-1748. doi:10.1038/s41588-019-0532-6
688 63. Dobin A, Davis CA, Schlesinger F, et al. STAR: ultrafast universal RNA-seq aligner.
689 *Bioinformatics*. Jan 01 2013;29(1):15-21. doi:10.1093/bioinformatics/bts635
690 64. Patro R, Duggal G, Love MI, Irizarry RA, Kingsford C. Salmon provides fast and bias-
691 aware quantification of transcript expression. *Nat Methods*. Apr 2017;14(4):417-419.
692 doi:10.1038/nmeth.4197
693 65. Revkov E, Kulshrestha T, Sung KW-K, Skanderup AJ. Accurate pan-cancer tumor
694 purity estimation from gene

695 expression data. 2022;doi: https://doi.org/10.1101/2022.06.01.494462
696 66. Yoshihara K, Shahmoradgoli M, Martínez E, et al. Inferring tumour purity and stromal
697 and immune cell admixture from expression data. *Nat Commun*. 2013;4:2612.
698 doi:10.1038/ncomms3612
699 67. Favero F, Joshi T, Marquard AM, et al. Sequenza: allele-specific copy number and
700 mutation profiles from tumor sequencing data. *Ann Oncol*. Jan 2015;26(1):64-70.
701 doi:10.1093/annonc/mdu479
702 68. Larson NB, Fridley BL. PurBayes: estimating tumor cellularity and subclonality in
703 next-generation sequencing data. *Bioinformatics*. Aug 01 2013;29(15):1888-9.
704 doi:10.1093/bioinformatics/btt293
705 69. Liu Y, Sethi NS, Hinoue T, et al. Comparative Molecular Analysis of Gastrointestinal
706 Adenocarcinomas. *Cancer Cell*. 04 09 2018;33(4):721-735.e8.
707 doi:10.1016/j.ccell.2018.03.010
708 70. Bindea G, Mlecnik B, Hackl H, et al. ClueGO: a Cytoscape plug-in to decipher
709 functionally grouped gene ontology and pathway annotation networks. *Bioinformatics*. Apr
710 15 2009;25(8):1091-3. doi:10.1093/bioinformatics/btp101
711

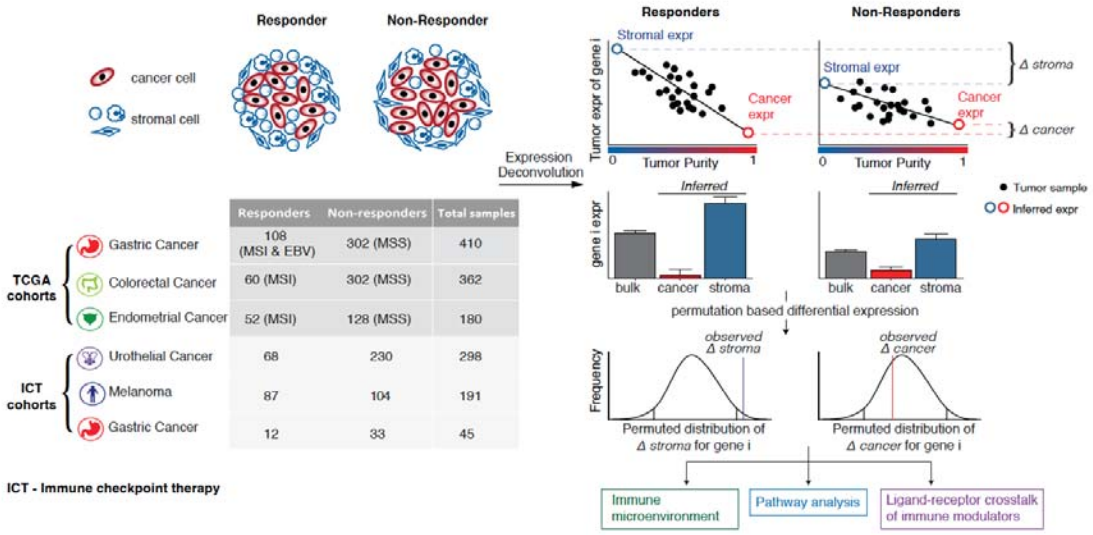

		Responders	Non-responders	Total samples
TCGA cohorts	Gastric Cancer	108 (MSI & EBV)	302 (MSS)	410
	Colorectal Cancer	60 (MSI)	302 (MSS)	362
	Endometrial Cancer	52 (MSI)	128 (MSS)	180
ICT cohorts	Urothelial Cancer	68	230	298
	Melanoma	87	104	191
	Gastric Cancer	12	33	45

Figure 1. Data summary and schematic of workflow for the analysis of determinants of immunotherapy response.

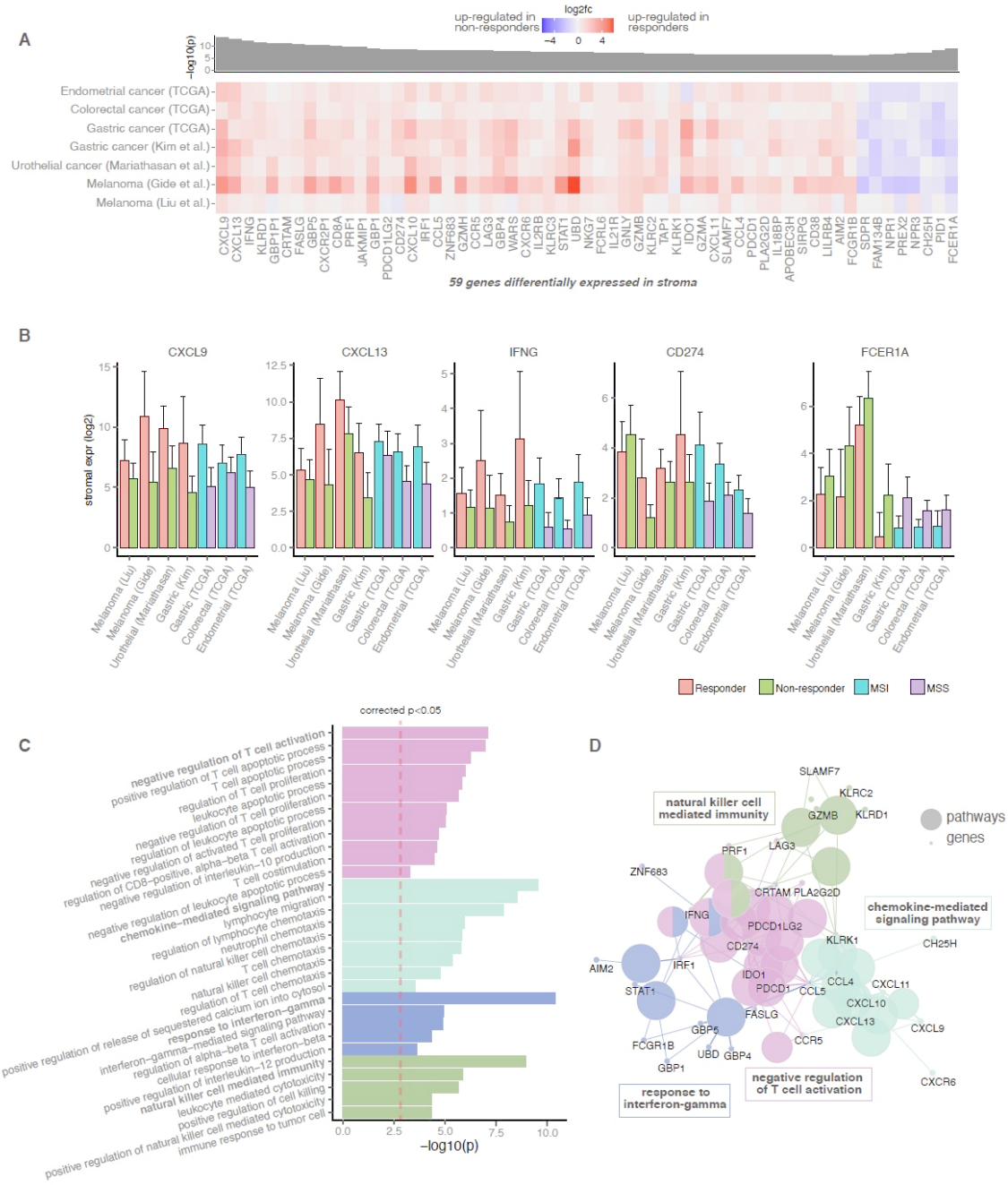

Figure 2. **Differentially expressed genes and pathways between responders and non-responders in the stroma. (A)** Heatmap of genes consistently differentially expressed across discovery cohorts in the stroma. Heatmaps are colored by the log2 fold change of gene expression. *P*-values of individual cohorts are combined using the Fisher's method, and the -log10(meta p-value) is presented in the bar plot. Genes with q-value<0.01 and *p*-value<0.1 at least 1 ICT cohort are shown. **(B)** Bar plots of deconvoluted stromal expression of the top differentially expressed genes. Error bars represent estimated standard error. **(C)** Pathway enrichment of differentially expressed genes in the stroma. Bar plot shows the -log10(p-value) of significantly enriched pathways. Similar pathways are grouped by color. (D)

Network representation of enriched pathways. Large nodes represent enriched pathways. Pathways with high similarity are fused and shown in the same color. Small nodes represent genes associated with each pathway.

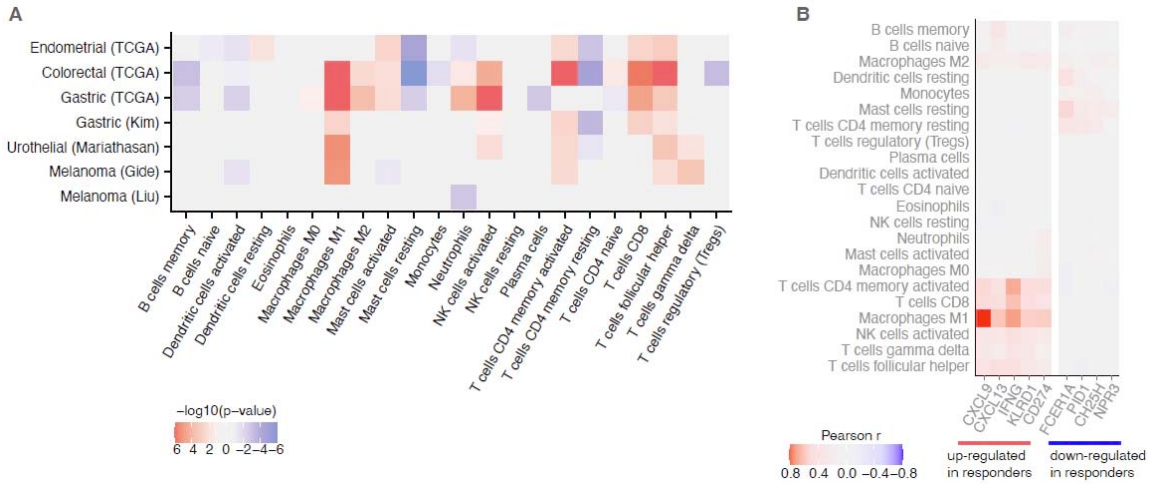

Figure 3. **Immune cell type enrichment analysis.** Abundance of immune cell types of each tumor is estimated using Cibersortx. **(A)** Heatmap of cell types analyzed. Heatmap is colored by the signed -log10(p-value) of the difference in Cibersortx scores between responders (MSI) and non-responders (MSS). **(B)** Correlations between the abundance of immune cell types with the gene expression of top stromal biomarkers.

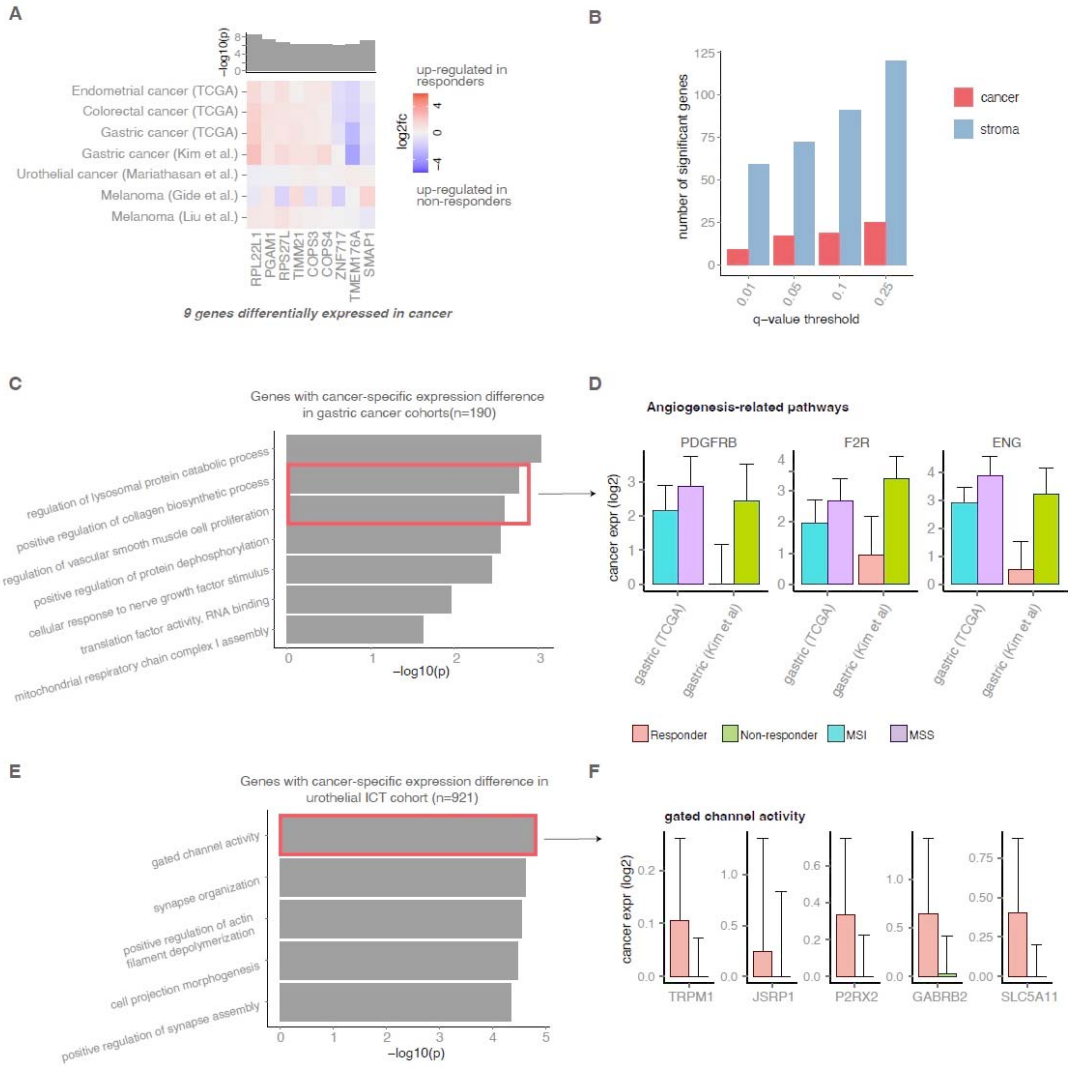

Figure 4. **Differentially expressed genes between responders and non-responders in the cancer compartment. (A)** Heatmap of genes consistently differentially expressed across discovery cohorts in the cancer cells. Heatmaps are colored by the log2 fold change of gene expression. *P*-values of individual cohorts are combined using the Fisher's method, and the -log10(meta p-value) is presented in the bar plot. Genes with q-value<0.01 and *p*-value<0.1 at least 1 ICT cohort are shown. **(B)** Bar plot shows the number of significant genes found in the stroma and cancer compartment at different q-value cutoffs. Pathway analysis of genes with cancer-specific expression differences in **(C)** gastric cancer and **(E)** urothelial cancer. Bar plots of deconvoluted cancer expression of differentially expressed genes in the top enriched pathway in **(C)** gastric cancer and **(E)** urothelial cancer. Error bars represent estimated standard error.

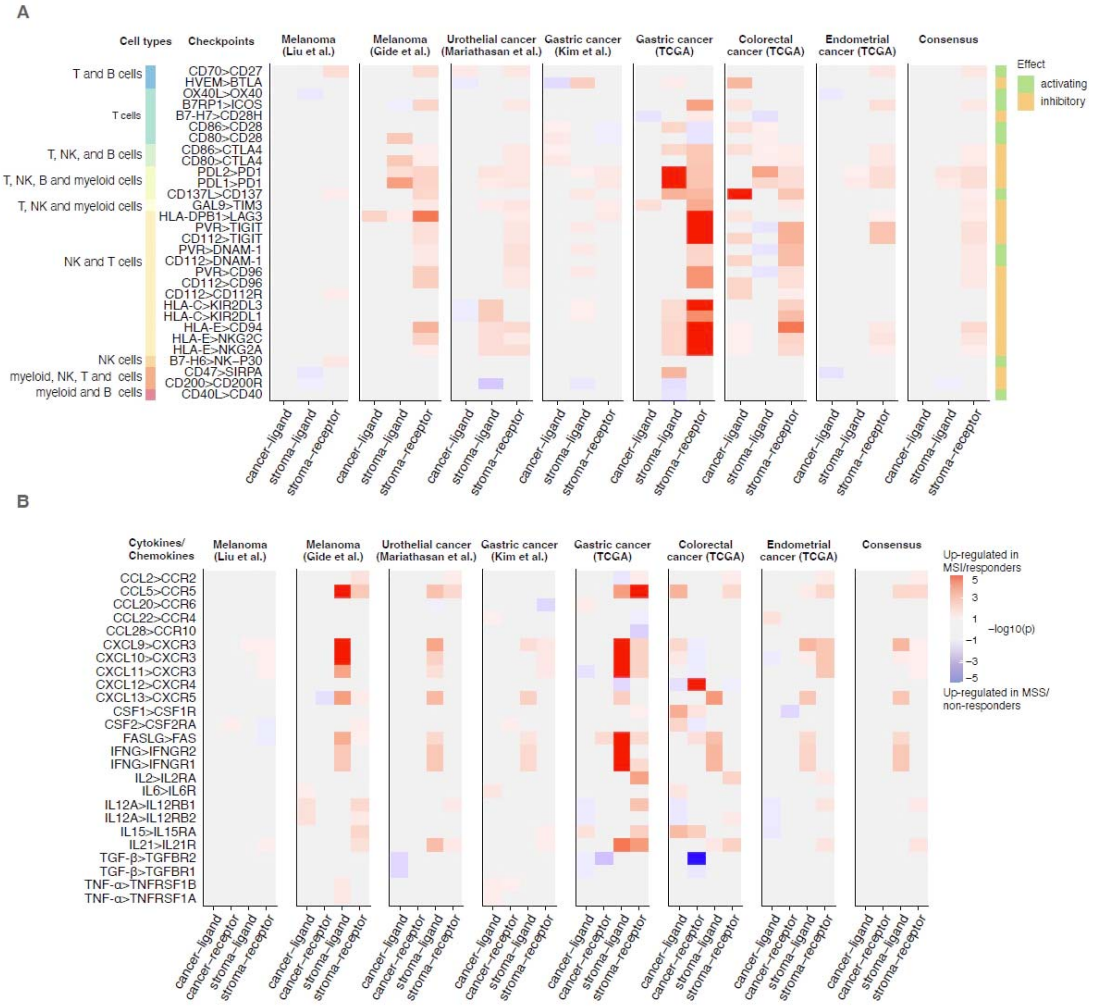

Figure 5. **Analysis of ligand and receptor expression of immune modulators.** Heatmaps of the inferred ligand and receptor expression in the cancer and stroma compartments for **(A)** immune checkpoint proteins and **(B)** cytokines. Heatmaps are colored by the signed -log10(*p*-value) of differential expression.

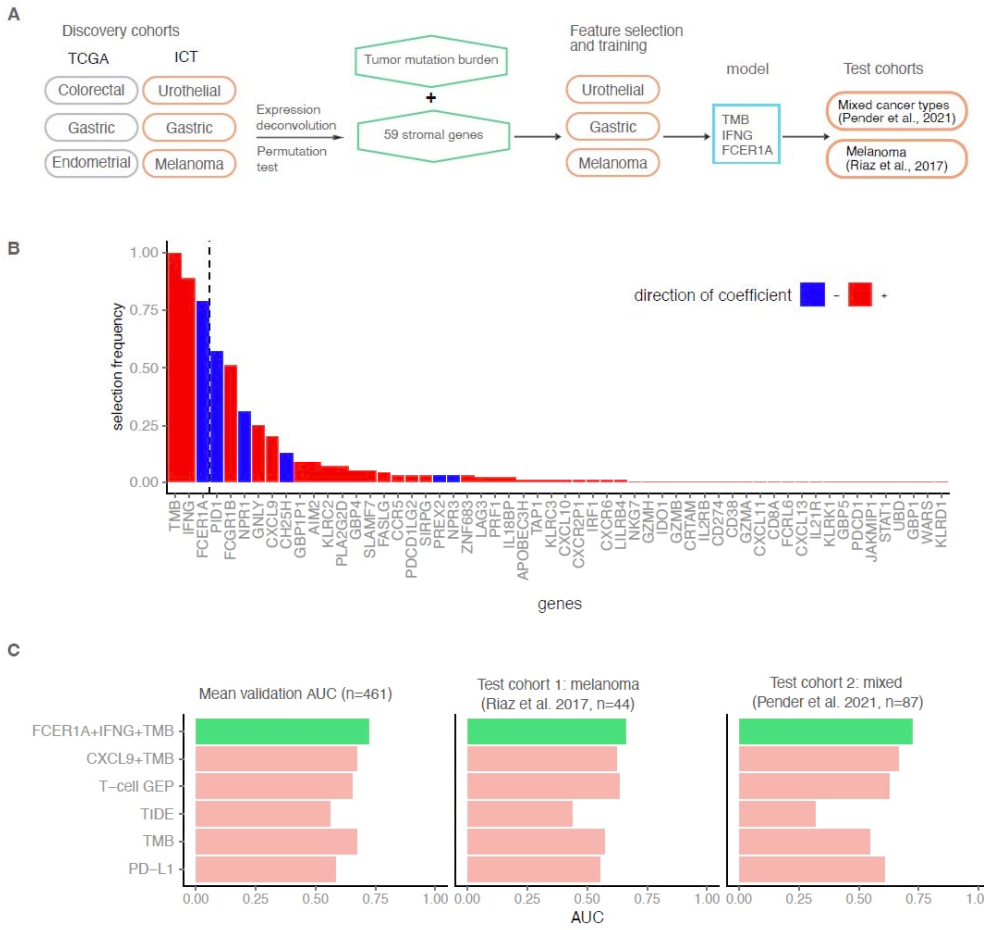

Figure 6. **Predictive modeling of response to immune checkpoint inhibition. (A)** Schematic of data and methods used in model training and testing. **(B)** Top ranked features of ICT response selected by LASSO logistic regression. **(C)** Comparisons of the performance of the TMB+*IFNG*+*FCER1A* model and existing biomarkers in 2 independent test cohorts.

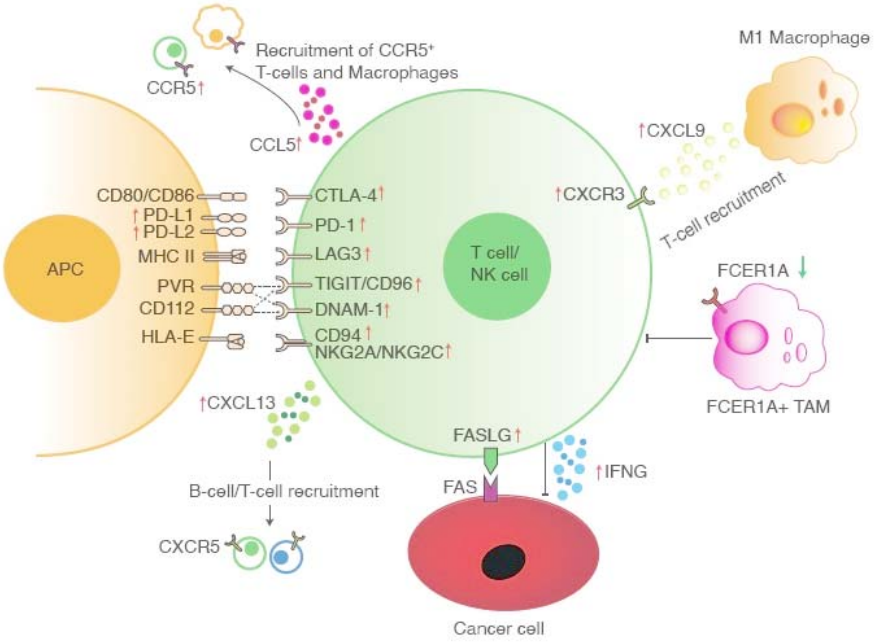

Figure 7. Schematic summarizing the key components associated with ICT response. Red arrows indicate gene positively correlated with ICT response. Green arrow indicates gene negatively correlated with ICT response.